ELSEVIER

Biophysical Chemistry 115 (2005) 235–240

Biophysical Chemistry

http://www.elsevier.com/locate/biophyschem

Dynamics of antibodies from cryo-electron tomography

L. Bongini[a,1], D. Fanelli[b,1], F. Piazza[c,*,1], P. De Los Rios[c], S. Sandin[b], U. Skoglund[b]

[a]*Centro Interdipartimentale per lo studio delle dinamiche complesse (CSDC) dell'Università di Firenze, Via G. Sansone 1, 50019 Florence, Italy*
[b]*Cell and Molecular Biology Department, Karolinska Institutet, 171 77 Stockholm, Sweden*
[c]*LBS-Institute de Physique Théorique, École Polytechnique Fédérale de Lausanne, BSP-720 CH-1015, Lausanne, Switzerland*

Received 25 June 2004; received in revised form 5 November 2004; accepted 10 December 2004
Available online 6 January 2005

Abstract

The issue of protein dynamics and its implications in the biological function of proteins are arousing greater and greater interest in molecular biology. In cryo-electron tomography experiments one takes several snapshots of a given biological macromolecule. In principle, a large enough collection of snapshots may then be used to calculate its equilibrium configuration in terms of the experimentally accessible degrees of freedom, and hence estimate its potential energy. Consequently, one could analyze the biological functions of biomolecules by directly accessing their dynamics.

In this work, we analyze the results of cryo-electron tomography experiments on monoclonal murine IgG2a antibodies. With the aid of a novel software for image processing, we measure the equilibrium distribution of the angles which describe the configuration of the molecule. This helps us shed some critical light on recent results from X-ray crystallography. We then build a model of the antibody dynamics, which enables us to use the measured angular distribution in order to derive an explicit expression of the IgG potential energy.

Finally, as a preliminary application of our results, we investigate the dynamical effects in the rate of formation of the antigen–antibody encounter complex. In particular, we suggest that the dynamics of antibodies operates in the direction of decreasing anticooperativity of the two antigen binding arms.

PACS: 87,15.He; 87.15.Vv; 82.39.-k 1
Keywords: Cryo-electron tomography; Antibodies; Statistical mechanics; Dynamics; Encounter rate; Anticooperativity

1. Introduction

It is now recognized that proteins are flexible dynamical systems, and exist in populations of different structures, rather then in a single rigid conformation. In fact, collective motions of domains greatly enhance proteins' ability to bind other molecules [1].

Antibodies link antigens and immunological effectors via highly mobile linkers that connect the hyper-variable antigen-binding sites to the effector domain (Fc). Remarkably, antibodies possess the structural flexibility to adapt to a huge variety of antigen shapes and sizes, while sharing similar conserved Fc regions that interact with a limited number of effector systems, such as Fc receptors and complement [2,3].

The antibody immunoglobulin G (IgG) is a glycoprotein with a molecular weight of 150 kDa, which binds to foreign agents, such as proteins on viruses' capsids, by subunits named fragment antigen binding arms (known as "Fabs" arms). Hinges connect two Fab arms to a stem that crystallizes easily ("Fc" stem), so that each antibody can bind to two antigens or to a single antigen with increased strength. It is known that the arms of the uncomplexed IgGs are highly flexible, with a wide range of variability of the reported values of Fab–Fab and Fab–Fc angles [4].

AFM spectroscopy, two-dimensional electron microscopy (EM) and physiochemical experiments also support a hypothesis of inherent flexibility of the IgG molecules [5,4,6]. However, there exists a great variability in the

* Corresponding author. Tel.: +412 169 305 13; fax:+412 169 305 23.
E-mail address: francesco.piazza@epfl.ch (F. Piazza).
[1] These authors contributed equally to the work.

0301-4622/$ - see front matter © 2004 Elsevier B.V. All rights reserved.
doi:10.1016/j.bpc.2004.12.037

literature as to the average values of crucial structural parameters such as Fab–Fab and Fab–Fc angles [7]. Large-scale conformational differences have also been detected among three complete structures of intact and functional antibodies (subclasses human IgG1, murine IgG1 and murine IgG2a) solved by X-ray crystallography [8,7]. This is partly due to the high fragility of the IgG molecules and more generally to the limitations intrinsic to experimental techniques such as electron microscopy and X-ray analysis. As a matter of fact, electron micrographs are two-dimensional representations and necessarily present projected images, making interpretation in three dimensions very difficult. On the other hand, X-ray crystallography suffers from the inherent ambiguities associated with unpredictability of differential packing environments within the crystals.

Electron tomography (ET) is a general method for three-dimensional reconstruction of individual objects from a tilt series of electron microscope images of a sample quenched to the temperature of liquid nitrogen [9–12]. As a result, one gets a *gallery* of instantaneous snapshots of the system. The ET technique can be applied to any transparent object [13–15] and it is not restricted to symmetrical or regularly arranged systems [16–18] or to objects with a preferred orientation on a support grid [19,20].

Recently, data from Cryo-ET of individual IgG molecules in solution have been analyzed with the aid of the powerful de-noising algorithm COMET, and confirmed that the position of the Fab arms relative to the Fc stem may greatly differ from one molecule to another [10]. Remarkably, it has been shown how the equilibrium statistics of the principal structural parameters of an IgG molecule may be reconstructed from the same set of experiments, and used as the starting point for studying the dynamics of an individual immunoglobulin in solution [21].

In this paper, we review the results presented in [21]. Additionally, we present a first application of those results to the study of the formation of an antigen–antibody encounter complex. The presentation of our work is organized as follows. In Section 2 we introduce the mechanical model and briefly review the statistical analysis of the experimental tomograms which led us to an explicit expression of the IgG internal potential energy. In Section 3 we study the antigen–antibody encounter by incorporating the IgG dynamics into a simple model of diffusion-driven reaction. In Section 4 we briefly summarize our findings.

2. A mechanical model of antibodies: from a collection of tomograms to the dynamics

The phase space of a system with n degrees of freedom can be parameterized by a vector $(\boldsymbol{q}, \boldsymbol{p})$ of n generalized coordinates $(q_{1,\ldots},q_n)$ and n conjugate momenta $(p_{1,\ldots},p_n)$, containing the information about the system configuration and velocity, respectively. When the system is in equilibrium with a thermal bath at temperature T any point in the phase space can be occupied with a probability density

$$\rho(\boldsymbol{q},\boldsymbol{p}) = \frac{1}{Z(T)} \exp\left[-\frac{K(\boldsymbol{q},\boldsymbol{p}) + V(\boldsymbol{q})}{k_{\mathrm{B}}T} \right], \tag{1}$$

where K is the kinetic energy, V the system potential, k_{B} the Boltzmann constant and $Z(T)$ a temperature dependent normalization factor.

If the equilibrium probability density of a system is made accessible experimentally, it is in principle possible to invert Eq. (1) in order to extract information regarding the dynamical properties of the system. This is the case in Cryo-ET experiments, where a direct measure of the equilibrium distribution in the configuration space can be performed through a statistical analysis of an ensemble of different snapshots of the system. The equilibrium probability distribution in the configuration space results from the integration of Eq. (1) over the conjugate momenta p_i:

$$\rho(\boldsymbol{q}) = \frac{1}{Z(T)} \exp\left[-\frac{V(\boldsymbol{q})}{k_{\mathrm{B}}T} \right] S(\boldsymbol{q}), \tag{2}$$

where

$$S(\boldsymbol{q}) = \int \exp\left[-\frac{K(\boldsymbol{q},\boldsymbol{p})}{k_{\mathrm{B}}T} \right] dp_1..dp_n. \tag{3}$$

The function $S(\boldsymbol{q})$ is the kinetic contribution to the equilibrium probability density and must be computed analytically. Once this is done, we can calculate the potential V as:

$$V(\boldsymbol{q}) = -k_{\mathrm{B}}T \ln\left[\frac{\rho(\boldsymbol{q})}{S(\boldsymbol{q})} \right] + V_0(T). \tag{4}$$

where $V_0(T)$ is a constant, which only depends on temperature. The temperature T in Eq. (4) characterizes the thermal equilibrium which describes the ensemble of individual snapshots. For any purpose, it is safe to assume 228 K<T<300 K [21].

In our model, we consider the immunoglobulin molecule to be composed of three rigid rods freely jointed together in a common point (Fig. 1): two (Fab) arms of equal mass M and length L and the (Fc) stem (pictorially, it may be visualized as a *lobster*). We choose to parameterize the configurational space of the system with the angles (ϕ_1,ϕ_2,θ). In this case, the mathematical derivation of the Hamiltonian is straightforward and we get [21]:

$$V(\phi_1,\phi_2,\theta) = -k_{\mathrm{B}}T \ln\left[\frac{\rho(\phi_1,\phi_2,\theta)}{\sin\phi_1 \sin\phi_2} \right], \tag{5}$$

where we have dropped the temperature-dependent additive constant.

The statistical distribution of the internal coordinates may be obtained directly from the three-dimensional reconstructions of individual molecules in solution. A

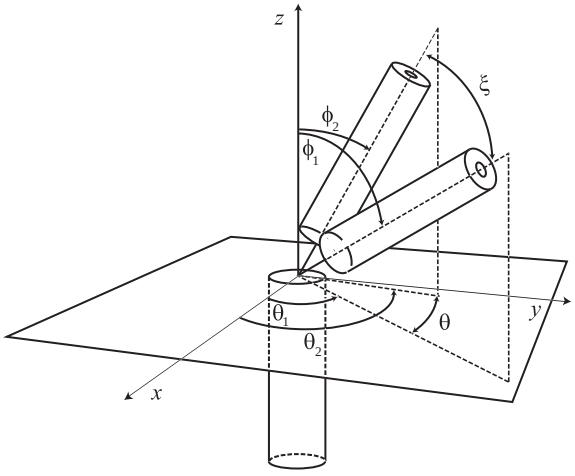

Fig. 1. Coarse-grained model of an immunoglobulin molecule. The two Fab arms and the Fc are replaced by rigid rods, freely jointed in the hinge region. The relative position of the $Fab_{1,2}$–Fc arms is described by the two angles ϕ_i and θ_i (i=1,2), in the Fab_i–Fc planes and in the plane perpendicular to Fc, respectively. The angle ξ measures the Fab–Fab separation in the Fab–Fab plane. Copyright (2004) National Academy of Sciences, USA.

typical gallery of individual, COMET-refined IgG structures is shown in Fig. 2 (for the details of the experiment and of the reconstruction technique see [10]).

The analysis of the reconstructed volumes allowed us to isolate 42 reliable structures of individual molecules. For each molecule, we measured the Fab–Fab angle ξ and the two Fab–Fc angles ϕ_1, ϕ_2, by approximating the three domains with ellipsoidal envelopes and measuring the angles formed by their major axes. The angle θ may then be obtained by straightforward trigonometry. Unfortunately, we have enough statistics to only access the coordinate space ϕ_1, ϕ_2, θ one angle at a time. Furthermore, we are not able to distinguish between the two Fab domains. Consequently, each molecule contributes two values to the population of the Fab–Fc ϕ angles. Accordingly, we assume that the density ρ (ϕ_1,ϕ_2,θ) can be factorized as the product of three one-dimensional normalized functions, namely $\rho(\phi_1,\phi_2,\theta)=\rho_1(\phi_1)\rho_1(\phi_2)\rho_2(\theta)$.

We show in Fig. 3 the normalized histogram of the experimental data $\rho_1(\phi)$ with $\phi_1=\phi_2=\phi$(upper panel), and the normalized experimental histogram $\rho_2(\theta)$ (lower panel). We find that the histogram of the Fab–Fc angles can be satisfactorily fitted with a uniform distribution in the interval [$\phi_{\min}$, $\phi_{\max}$], with $\phi_{\min}\approx 15^\circ$ and $\phi_{\max}\approx 127{:}6^\circ$, namely

$$\rho_1(\phi)=\begin{cases}\frac{1}{\phi_{\max}-\phi_{\min}} & \phi_{\min}<\phi<\phi_{\max}\\ 0 & \text{otherwise}\end{cases}. \qquad (6)$$

The θ angles are measured in the interval [0, 180°], since we cannot systematically identify the front and back broad sides of the Fc domain in the reconstructed data. Therefore, in order to extend the distribution domain to the interval [180°, 360°], we perform a reflection of the data around θ=180°. The experimental data show then clearly a symmetric bell-shaped function, peaked at θ=180°. This means that the configurations with both Fabs lying in the plane passing through the Fc stem are the most probable ones. We find that a simple Lorentzian profile truncated in [0, 360°] fits the data extremely well:

$$\rho_2(\theta)=\frac{1}{2\sigma_\theta \operatorname{atan}(\theta_0/\sigma_\theta)}\left[1+\left(\frac{\theta-\theta_0}{\sigma_\theta}\right)^2\right]^{-1} \qquad (7)$$

where θ_0=180°, and σ_θ is the only floating parameter. From the fit we find $\sigma_\theta\approx 91.6^\circ$.

We are now able to compute the effective potential energy V (ϕ_1, ϕ_2, θ). By using the factorization hypothesis,

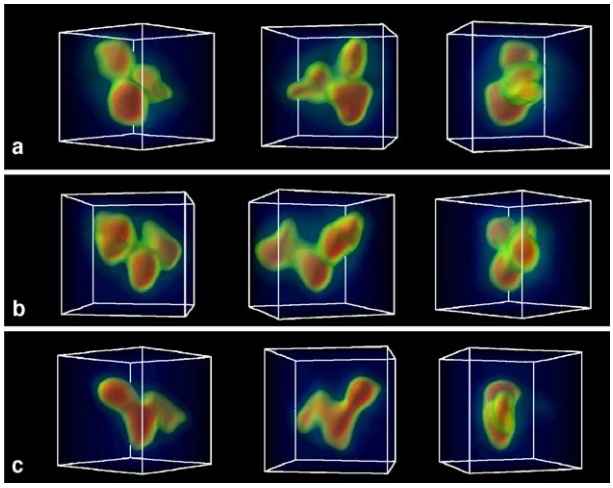

Fig. 2. Gallery of individual IgG molecules, visualized by volume rendering in three dimensions. Three different views of each tomograms are displayed. The box is 50×40×50 pixels (1 pixel=5.24 A). Copyright (2004) National Academy of Sciences, USA.

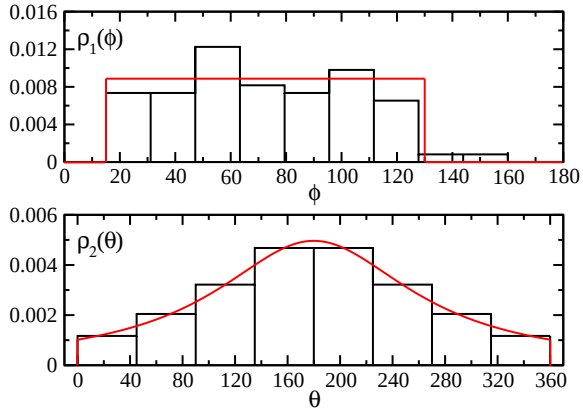

Fig. 3. Upper panel: normalized histogram of the experimental ϕ angles and plot of the square function (6) with $\phi_{\min}\approx 15^\circ$ and $\phi_{\max}\approx 127.6^\circ$. Lower panel: normalized histogram of the experimental θ angles and plot of the truncated Lorentzian (7) with $\sigma_\theta\approx 91.6^\circ$.

and expressions (6) and (7), Eq. (5) can be written as a sum of three terms, $V(\phi_1, \phi_2, \theta)=V_1(\phi_1)+V_1(\phi_2)+V_2(\theta)$, where

$$V_1(\phi) = k_B T[\ln(\sin\phi)]$$

$$V_2(\theta) = k_B T \ln\left[1 + \left(\frac{\theta - \theta_0}{\sigma_\theta}\right)^2\right]. \quad (8)$$

The interested reader can find an extensive discussion of the above potential energy in [21], along with a critical view on the difficult task of determining the value of the temperature T. Here, we shall rather focus on the implications of the potential energies (Eq. (8)) on the average conformations of an immunoglobulin, with emphasis on the peculiar interconnections among dynamics, conformation and encounter efficiency.

We have found that the two Fab arms most likely lie within the same plane as the Fc, although with substantial statistical weight assigned to off-plane configurations.

The statistical bias toward planar Y-like configurations introduced by the potential energies (Eq. (8)), albeit small, is enough to determine an average Fab–Fab angular separation 10% greater than in the unbiased case, i.e. when $V_1(\phi)=V_2(\theta)$=constant. The latter scenario would describe a pair of free Fabs, and we take it here as reference to investigate the role of the potential energies $V_1(\phi)$ and $V_2(\theta)$. In this case one would have $\rho_2(\theta)$=constant, $\rho_1(\phi) \propto \sin\phi$ (see Eq. (5) and (8)). This effect is represented in Fig. 4, where we show the experimental histogram $\rho_3(\xi)$ of the Fab–Fab angles ξ, along with numerical predictions of the biased and unbiased scenarios. That is, histograms from populations of random ξ angles generated from the corresponding distributions $\rho_1(\phi)$ and $\rho_2(\theta)$. It is obvious that the unbiased scenario does not capture the statistics of Fab–Fab angles, while the one-dimensional distributions (6) and (7) seem to nicely reconstruct the experimental histogram $\rho_3(\xi)$. Incidentally,

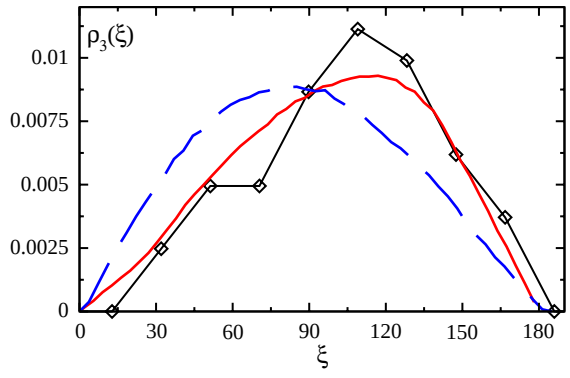

Fig. 4. Statistical distribution of the Fab–Fab angles. Thin solid line with symbols: experimental histogram. Thick solid line: simulation according to the experimental distributions of the θ and π angles. Thick dashed line: unbiased scenario (see text).

we observe that the latter conclusion can be considered an a posteriori validation of our factorization hypothesis $\rho(\phi_1, \phi_2, \theta)=\rho_1(\phi_1)\rho_1(\phi_2)\rho_2(\theta)$. From the experiments we get $\langle\xi\rangle \approx 104^\circ \pm 6^\circ$. Conversely, free motion of the Fabs results in $\langle\xi\rangle \approx 91.7^\circ$.

3. Anticooperativity in the encounter of antigens and antibodies: a dynamical view

As a first application of our results, we wish to study the rate of encounter between an antibody and an antigen of given size.

Nature has provided antigen seekers with two binding arms. This means that immunoglobulins will bind more than single-Fab analogs. However, the two chasers will interact against each other, thus diminishing the overall rate with respect to what pure additivity would predict. How relevant is, if any, this anticooperative effect?

We argue that antigens which are smaller in size with respect to the Fab arms will see antibodies in a first approximation as pairs of active centers separated by a fixed distance d. In particular, they will see a *static* distribution of such distances $P(d)$, which will depend on the antibody internal dynamics. Accordingly, we expect the anticooperative effects to depend on the distribution $P(d)$.

We wish to construct a simple model of diffusion driven encounter between the immunoglobulin and a small antigen, in order to investigate the effects of the internal dynamics on the anticooperativity. To this end, we model the antigen as a sphere of radius R_1, and the IgG as a pair of spheres $S^{\pm}$ of radius R_2, fixed at a distance d. Let $\boldsymbol{r}$ indicate the position vector of the antigen with respect to the center of mass of the two spheres. If we neglect rotation and time-dependent effects, our problem reduces to finding the stationary solution of the following Laplace problem for the concentration of antigens $c(\boldsymbol{r})$

$$\nabla^2 c(\boldsymbol{r}) = 0$$

$$c|_{S^+} = c|_{S^-} = 0$$

$$\lim_{\boldsymbol{r}\to\infty} c(\boldsymbol{r}) = c_\infty \quad (9)$$

where c_∞ is the antigen bulk concentration and we impose absorbing boundary conditions on the surface of the system $S^+ + S^-$. Let D_1 and D_2 be the antigen and IgG diffusion coefficients, respectively. The encounter rate constant can be calculated by evaluating the flux of antigens across any closed surface Ω enclosing the sinks

$$k = D^* \Phi(c) = D^* \int_\Omega \vec{\nabla} c \cdot \hat{\boldsymbol{n}}\, dS \quad (10)$$

where $D^*=D_1+D_2/2$.

The problem (9) may be solved by adopting the bispherical coordinate set. The details of the calculations are reported in a more complete paper [22]. We obtain

$$\kappa = 2\kappa_S\sqrt{\chi^2-1}\sum_{n=0}^{\infty}\frac{2}{1+\left[\chi+\sqrt{\chi^2-1}\right]^{2n+1}} \tag{11}$$

where $\chi=d/2d_e>1$, $d_e=R_1+R_2$ is the encounter distance and $\kappa_S=4\pi D^*(R_1+R_2)$. At this point, a quantitative measure of anticooperativity may be introduced through the following simple indicator

$$\mathcal{A}(d,R_1)=\frac{\kappa}{2\kappa_1}-1 \tag{12}$$

where we have explicitly indicated the dependence on the Fab–Fab distance d and antigen radius R_1. The quantity $\kappa_1=4\pi(D_1+D_2)(R_1+R_2)$ is the Smoluchowski rate constant describing the encounter of the antigen with a single, isolated Fab sphere.

The function $\mathcal{A}(d, R_1)$ is a monotonously decreasing function of the antigen radius R_1 for fixed Fab–Fab separation d, and a monotonously increasing function of d at fixed R_1. This means that the configurations of the IgG with the largest Fab–Fab distances will produce the smallest contributions to the average anticooperativity. In the formal limit of infinite separation between active centers $d\to\infty$, it is not difficult to realize that $\lim_{d\to\infty}\kappa=2\kappa_S$. Consequently, additivity is nearly recovered for small antigens in that limit, as

$$\lim_{d\to\infty}\mathcal{A}(d,R_1)=-\frac{D_2}{2(D_1+D_2)}\approx-\frac{R_1}{2R_2}\ll 1$$

where we have used the Einstein rule $D_i\propto 1/R_i$, i=1, 2. In the opposite limit $d\to 2d_e$ (or equivalently $\chi\to 1$), anticooperativity attains its maximum. In this case $\lim_{\chi\to 1}\kappa=2\kappa_S\log(2)$ [22], and hence

$$\lim_{d\to 2d_e}\mathcal{A}(d,R_1)=\frac{2R_2+R_1}{2(R_2+R_1)}\log(2)-1\approx\log(2)-1.$$

The average anticooperativity in the limit of small antigens may be obtained by averaging over the static distribution of distances, which may be easily obtained numerically in the same fashion as the distributions of the ξ angles

$$\langle\mathcal{A}(R_1)\rangle=\int_{2d_e}^{2L}\mathcal{A}(x,R_1)P(x)dx. \tag{13}$$

It is clear that the two Fabs have a marked tendency to stay farther apart in the biased scenario with respect to the free, unbiased case (Fig. 5a). We may then speculate that the presence of the potential energies (8) reflects the effort of keeping the two Fabs away from each other. This inference is supported by the analysis of the average anticooperativity.

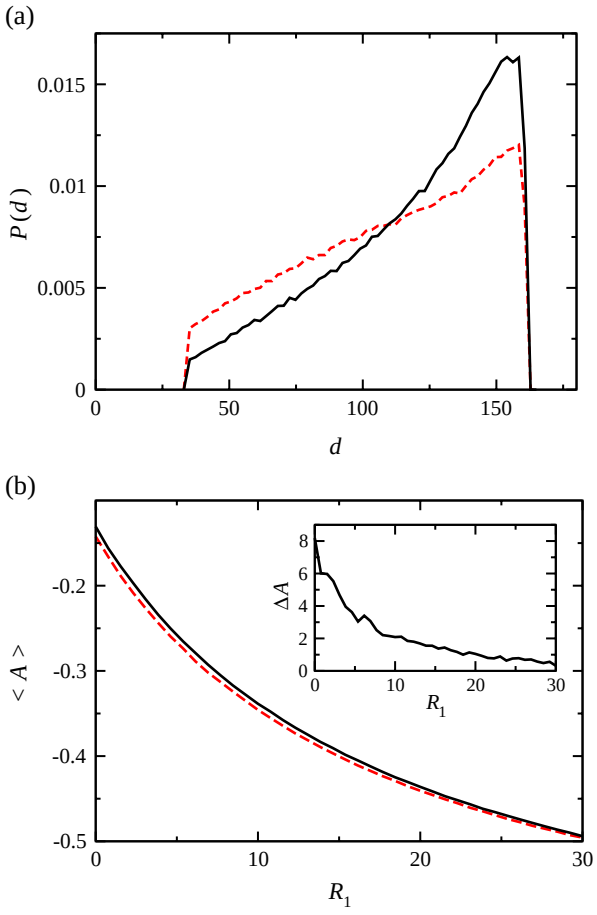

Fig. 5. (a) Numerical histograms of Fab–Fab distances. Solid curve, distribution generated according to the experimental distributions $\rho_1(\phi)$ and $\rho_2(\phi)$ (biased case). Dashed curve, unbiased case [$V_1(\phi)=V_2(\theta)$=constant]. The cutoff $d>2R_2$ has been introduced in the computation of the histograms. The parameter R_2 has been fixed at R_2=16.5 Å, which is the value that reproduces the observed domain of Fab–Fc angles [ϕ_{min}, ϕ_{max}], for an IgG of radius L=80 Å with a spherical Fc of radius 34.4 Å. (b) Plot of the average anticooperativity (12) as a function of the antigen radius. The solid curve is calculated by averaging over the distribution $P(d)$ in the biased case. The dashed curve is the average anticooperativity in the unbiased case. Inset: relative difference of the two anticooperativities (14) (percent). Distances are measured in Å.

Our results indicate that for small antigens the anticooperative effect may decrease the encounter rate of as much as 30% (Fig. 5b). We recall that we expect our assumptions to be less accurate for antigens of size comparable to that of the two Fabs. However, we see that the absence of a bias in the Fab–Fab relative orientation due to the presence of the potential energies may increase the anticooperativity effect up to 5–6%. This tendency is shown quantitatively in the inset of Fig. 5b, where we plot the relative difference

$$\Delta\mathcal{A}=1-\frac{\langle\mathcal{A}_{pot}\rangle}{\langle\mathcal{A}_{free}\rangle}. \tag{14}$$

The two pedices refer to the average anticooperativity in the biased (pot) and unbiased (free) scenarios.

Summarizing, we speculate that the potentials would reduce *negative interference* between the two binding arms in the diffusion-controlled encounter with antigens by favoring large values of the Fab–Fab separation.

4. Conclusions

In this paper we have shown that high-resolution tomographic reconstructions of individual immunoglobulins in solution may be analyzed to investigate the equilibrium conformations of the molecules. Our results clearly show that, especially for large, flexible macromolecules, the number of different conformations adopted may dramatically differ from the results of X-ray crystallography or of other techniques based on structural averaging such as single-particle tomography.

Importantly, the results of an accurate statistical analysis of individual structures may be used to compute an effective internal potential energy of the molecule through standard tools of equilibrium statistical mechanics. This, in turn, may open the way to a direct *dynamical* investigation of different biological functions of the molecule. For example by means of Langevin simulations.

As a first application, we have shown that the bias in the relative orientation of the two Fab arms introduced by the experimental potential energies increases on average the statistical weight assigned to large Fab–Fab separations. Consequently, it operates in the direction of reducing the anticooperative effects in the diffusion-driven encounter of the Fabs with antigens of small size.

References

[1] P.W. Fenimore, H. Frauenfelder, B.H. McMahon, F.G. Parak, Slaving: solvent fluctuations dominate protein dynamics and functions, Proc. Natl. Acad. Sci. U. S. A. 99 (25) (2002) 16047.
[2] D.R Burton, Immunoglobulin-G functional sites, Mol. Immunol. 22 (1985) 161.
[3] D.R. Burton, Antibody the flexible adapter molecule, Trends Biochem. Sci. 15 (1990) 64.
[4] K. Roux, Immunoglobulin structure and function as revealed by electron microscopy, Int. Arch. Allergy Immunol. 120 (1999) 85.
[5] F. Kienberger, H. Mueller, V. Pastushenko, P. Hinterdorfer, Following single antibody binding to purple membranes in real time, EMBO Rep. 5 (6) (2004) 579.
[6] R. Nezlin, Internal movements in immunoglobulin molecules, Adv. Immunol. 48, 1.
[7] E.O. Saphire, R.L. Stanfield, M.D. Max Crispin, P.W.H.I. Parren, P.M. Rudd, R.A. Dwek, D.R. Burton, I.A. Wilson, Contrasting IgG structures reveal extreme asymmetry and flexibility, J. Mol. Biol. 319 (2002) 9.
[8] L.J. Harris, S.B. Larson, E. Skaletsky, A. McPherson, Comparison of the conformations of two intact monoclonal antibodies with hinges, Immunol. Rev. 163 (1998) 35.
[9] U. Skoglund, K. Andersson, B. Strandberg, B. Daneholt, 3-Dimensional structure of a specific pre-messenger RNP particle established by electron-microscope tomography, Nature 319 (1986) 560.
[10] S. Sandin, L.-G. Öfverstedt, A.-C. Wikström, Ö. Wrange, U. Skoglund, Structure and flexibility of individual immunoglobulin G molecules in solution, Structure 12 (3) (2004) 409.
[11] P.F.C. Gilbert, Reconstruction of a 3-dimensional structure from projections and its applications to electron microscopy—2. Direct methods, Proc. R. Soc. Lond., B 182 (1972) 89.
[12] W. Hoppe, J. Gassmann, N. Hunsmann, J. Schramm, M. Sturm, 3-Dimensional reconstruction of individual negatively stained yeast fatty-acid synthetase molecules form tilt series in electron-microscope, Hoppe-Seyler Z. physiol. Chem. 355 (1974) 1483.
[13] U. Skoglund, B. Daneholt, Electron-microscope tomography, Trends Biochem. Sci. 11 (1986) 499.
[14] J. Frank, Approaches to large-scale structures, Curr. Opin. Struck. Biol. 5 (1995) 194.
[15] U. Skoglund, L.-G. Öfverstedt, B. Daneholt, RNP Particles, Splicing and Autoimmune Diseases, in: J. Schenkel (Ed.), 1997. Springer Lab Manual, Springer Verlag, Heidelberg, pp. 72–94.
[16] D.J. De Rosier, A. Klug, Reconstruction of 3-dimensional structures from electron micrographs, Nature 217 (1968) 130.
[17] R.A. Crowther, D.J. De Rosier, A. Klug, Reconstruction of a 3-dimensional structure from projections and its application to electron microscopy, Proc. R. Soc. Lond., A 317 (1970) 319.
[18] D.J. De Rosier, P.B. Moore, Reconstruction of 3-dimensional images from electron micrographs of structures with helical symmetry, J. Mol. Biol. 52 (1970) 355.
[19] M. Radermacher, T. Wagenknecht, A. Verschoor, J. Frank, 3-Dimensional reconstruction from a single-exposure, random conical tilt series applied to the 50S-ribosomal subunit of *Escherichia-coli*, J. Microsc. 146 (1987) 113.
[20] M. Radermacher, 3-Dimensional reconstruction from a single particles from random and nonrandom tilt series, J. Electron Microsc. Tech. 9 (1988) 359.
[21] L. Bongini, D. Fanelli, F. Piazza, P. De Los Rios, S. Sandin, U. Skoglund, Freezing immunoglobulins to see them move, Proc. Natl. Acad. Sci. 101 (2004) 64661.
[22] F. Piazza, L. Bongini, D. Fanelli, P. De Los Rios, Eur. Biophys. J. (2004) (in press).